ARL-TR-2

AR-007-113

DEPARTMENT OF DEFENCE

DEFENCE SCIENCE AND TECHNOLOGY ORGANISATION

AERONAUTICAL RESEARCH LABORATORY

MELBOURNE, VICTORIA

Technical Report 2

FIELD EVALUATION OF SIX PROTECTIVE COATINGS APPLIED TO T-56 TUBINE BLADES AFTER 2000 HOURS OF ENGINE USE

by

S.G. RUSSO

Approved for public release.

NOVEMBER 1992

DISCLAIMER NOTICE

THIS DOCUMENT IS BEST QUALITY AVAILABLE. THE COPY FURNISHED TO DTIC CONTAINED A SIGNIFICANT NUMBER OF COLOR PAGES WHICH DO NOT REPRODUCE LEGIBLY ON BLACK AND WHITE MICROFICHE.

DEPARTMENT OF DEFENCE
DEFENCE SCIENCE AND TECHNOLOGY ORGANISATION
AERONAUTICAL RESEARCH LABORATORY

Technical Report 2

FIELD EVALUATION OF SIX PROTECTIVE COATINGS APPLIED TO T-56 TUBINE BLADES AFTER 2000 HOURS OF ENGINE USE

by

S.G. RUSSO

SUMMARY

The first-stage high-pressure turbine blades in RAAF T-56 engines have a rejection rate which is unacceptably high. It has been revealed [1] that the current coating, a conventional nickel aluminide, has a greater than 60% rejection rate after 2000 hours. Consequently, a trial programme was established to assess the benefits of five alternative protective coatings and to determine which coatings, if any, could withstand up to 3000 engine operating hours. A previous report demonstrated the potential of platinum and platinum/rhodium modified aluminides after 1500 hours of engine operation. This report, after approximately 2000 hours of service, supports the previous recommendations that the precious metal aluminides offer superior resistance to hot corrosion than the conventional aluminides and chromium-modified aluminides. The inability of the silicon-modified aluminide to form an evenly distributed coating over the entire blade renders it unsuitable.

DSTO AUSTRALIA

POSTAL ADDRESS: Director, Aeronautical Research Laboratory
506 Lorimer Street, Fishermens Bend 3207
Victoria Australia

CONTENTS

1. INTRODUCTION

The current aluminide coating applied to the fleet of RAAF T56-A-14 engines has been suffering from a combination of oxidation and hot corrosion.* Two different forms of hot corrosion have been identified. Type I High Temperature Hot Corrosion (HTHC), which is present over a range of about 800-950°C, and Type II Low Temperature Hot Corrosion (LTHC), which occurs over the temperature range 650-800°C. Consequently, a trial programme was established to investigate the performance of the current coating against five other coating systems applied to the T56 turbine blades. The coating systems consisted of (i) two nickel aluminides designated A and B; (ii) a platinum-modified aluminide; (iii) an aluminide modified with platinum and rhodium; (iv) a chromium-modified aluminide and (v) a silicon-modified aluminide applied using a slurry process. The T56 high pressure turbine (HPT) blades are manufactured from a vacuum cast nickel-base superalloy, designated IN-738LC, whose weight composition is shown in Appendix I. More information regarding the initial microstructure and processing methods of these coatings was given in a previous report [2].

This investigation deals with the performance of 12 turbine blades received from the RAAF Allison T56-A-14 engine (Serial No. 107409) after having experienced approximately 2000 hours of engine use. The report [2] based on these coatings after 1500 hours of engine use was previously published as Aircraft Materials Technical Memorandum 405, AR-006-615.

The previous report found that after 1500 hours of engine operation, the platinum, platinum/rhodium and to a lesser extent the silicon-modified coatings, offered superior resistance when compared to the chromium-modified aluminide and basic nickel aluminides. Other reports relating to hot corrosion from the engines in RAAF and RAN aircraft can be found elsewhere [3-6].

2. BLADE SURFACE FEATURES

2.1 Visual Inspection

Photographs of the concave side of each blade are shown in Figures 1 to 6. Areas of insignificant attack accompanied by areas of severe degradation were apparent. Corrosive attack appeared to be localised around the leading edge and concave faces. The convex surfaces, although experiencing somewhat less severe conditions than the concave surfaces,

* The term 'hot corrosion' is commonly used to describe acce erated low and high temperature corrosion caused by the presence of molten salts, abundant in sodium sulphate, on metal or oxide scale surfaces.

showed several areas of discolouration. In general, the convex side of the blades was free from any form of hot corrosion attack.

Visual examination of the variously coated T56 HPT blades indicated that the silicon-modified aluminide coating (Figure 1) appeared to suffer minimal surface attack. Some discrepancies appeared in the extent of degradation for the Aluminide A coatings (Figure 2). The first blade showed small areas of attack mid-way along the concave leading edge, while the degraded area on the second blade was a factor of 10 greater. The extensive attack on the leading edge in Figure 2(b) indicated that in this location, the coating was depleted and no longer protected the substrate. Blisters and severe penetration into the substrate were evident on this blade. The chromium-modified aluminide coated blades (Figure 3), although appearing to have a patchy-coloured surface, seemed to maintain their integrity as a protective coating. Both blades exhibited a narrow area of attack running the full length of the concave leading edge. The platinum-modified aluminide coating shown in Figure 4 illustrates severe corrosion but apparently it is only superficial. A clear explanation for this unexpected phenomenon will be resolved, hopefully, after detailed microanalysis. Evidence of severe scratching near the root platform, indicated by the arrows in Figure 5, were visible on the platinum/rhodium modified aluminide. This may well be explained by the presence of one of two common modes of blade impairment, namely foreign object damage (FOD) or erosion by hot particulate compounds. It was noted that the blade shown in Figure 5(b) contained other localised areas of attack which were not located on the susceptible leading edge. Figure 6 illustrates the Aluminide B coating. This contains surface features similar to those of Aluminide A, but some of the visual characteristics of these two blades were inconsistent with one another. However, the relative variations in degradation between the Aluminide B coatings was only a factor of 3.

Many of these photographs show discrepancies in observed surface attack between identical coatings. These differences are understandable, simply because there are so many variables influencing the life of an aluminide coating. For example, the position of any one blade in the turbine disc may determine its likelihood and degree to which it is subjected to an uncertain amount of molten salt. Thus unequivocal explanations are difficult to provide. The only common characteristic that was evident on every blade was the occurrence of a dark coloured compound near the root platform. The details of this are mentioned in the next section.

An estimate of surface spallation in the form of a bar chart for each of the coatings is illustrated in Figure 7. As presented in the previous report, several large variations in attack for identical coatings are obvious. It is important to mention the striking differences between the full and partly shaded bars for the platinum and platinum/rhodium modified aluminide coatings. However, these do not give a clear indication of the extent of spallation. The

reason for this being that, in these two cases, only superficial spallation of the oxide scale was found. Further details of this are discussed later.

In general, the maximum corrosive attack occurred on the concave section of the leading edge at the mid-span while the convex side exhibited only limited attack and moderate discolouration. Since every blade indicated varying degrees of attack at different locations, Table 1 was constructed to determine the overall performance of each aluminide coating to surface spallation.

2.2 X-Ray Spectroscopy

The first set of results obtained using X-Ray spectroscopy were carried out on each unsectioned blade prior to metallographic examination. Areas of each blade, both attacked and non-attacked regions, magnified 200 times, were analysed. The results are presented below. Typical qualitative X-Ray analyses of one of the blades is presented in Figure 8. In general, comparisons made of the attacked and non-attacked regions revealed the following information:

- nickel peaks were far greater in the attacked regions where the protective oxide layers had been breached, exposing the underlying β-NiAl phase and the innermost nickel oxide (NiO) scale.

- several blade surfaces exhibited areas of blistering resulting in the formation of 'craters'. X-Ray analyses of these areas indicated higher concentrations of phosphorous, sodium and silicon and to a lesser extent calcium, than would otherwise be expected. It must also be noted that the surface of these blistered regions did not contain any sulfur.

- zinc and iron, foreign elements in both the substrate and blade coating, probably owe their presence to component damage further up in the airstream. These elements were present, to a similar degree, in both the attacked and unattacked areas.

- phosphorous, present most likely as a calcium phosphate, was abundant in all regions of each of the turbine blade surfaces. Its presence is discussed in more detail later.

- the quantity of sodium present in any region appeared to be directly related to the corresponding amount of magnesium present. The degree to which these elements were present was greater in the unattacked regions than in the regions of corrosive attack.

- the high abundance of titanium, iron, magnesium, silicon, zinc, and calcium in regions that had not been degraded suggests they were very likely present in the form of oxides or sulphates.

- sulfur was present in every area of blade surface examined. Furthermore, it did not appear to be any greater in the degraded regions.**

- the higher concentration of potassium in the unattacked regions is another unexplainable feature of this X-Ray analysis.

The area scans can only be used as a guide to the presence of certain elements on the surface of the blade. The aim of this analysis was to determine the elements present on the surface and those that were not naturally occurring in either the substrate or the coating (eg. calcium, potassium, sulfur, sodium etc.). The likely origins of these foreign elements are explained in Table 2. The abundance of sodium, magnesium, calcium and sulfur re-affirms the most likely cause of hot corrosion being derived from ingestion of sea salt. Appendix II presents a typical chemical composition of sea salt.

2.3 X Ray Diffraction

Every blade examined exhibited an area of black deposition on the concave root platform as is shown in Figure 1. Two types of deposit were apparent, dark brown and light brown with the former occurring on badly attacked blades. Variations in the quantities of NiAl and Ni_2Al_3 within the deposits may explain their differences in colour. X-Ray Diffraction (XRD) was undertaken in the hope of learning some information about the type of environment the engine components had been subjected to. Results indicated a high amount of SiO_2, the prime constituent of sand, and smaller amounts of coating compounds, NiAl and Ni_2Al_3.

3. MICROSTRUCTURAL ANALYSES OF THE COATINGS

3.1 Blade Preparation Procedure

The procedure used for metallographic examination was similar to the previous report [2]. Blades were first coated with a carbon/epoxy resin, to reduce the degree of 'charging' in the electron microscope, followed by a gold sputter. In order to achieve good edge retention and to retain oxide scales and deposits, a nickel plate was applied to the blades using a nickel

** Sulfur is an unfavourable addition in the coating as it has the ability to form low m.p. sulfides and leads to a loss of adhesion in the Al_2O_3 scale [7].

sulphamate bath. Sectioning of the blades was performed at a length of approximately 14mm from the shroud root. This distance corresponded to a position where each blade had visually suffered extensive surface attack. Once the sections of the blade were mounted they were polished to a 1μm finish for microanalyses.

3.2 Coating Microscopy and Microanalysis

3.2.1 Leading Edge Microscopy

Six leading edge (LE) micrographs, one from each coating system, are shown in Figure 9. They clearly highlight the variations in attack between each of the different coatings. The concave region, shown on the left side of each micrograph, experiences a more severe degree of attack when compared with the convex side. Except for the platinum-modified aluminide coating, all the L.E. micrographs exhibited varying degrees of attack ranging from moderate to severe.

Although the silicon-modified aluminide coating did not show much evidence of oxide penetration, it demonstrated poor qualities in other areas. For example, the coating surface appeared very rough. Explanations for this may lie in the fact that the coating was applied by manually brushing the blade with a silicon containing slurry. Therefore, the quality of the coating was more dependant on the skill of the operator applying the coating. Moreover, silicon-modified coatings with their high ductile to brittle transition temperatures (DBTT) [8], are more prone to fail by brittle fracture than the other coatings examined.

Both the aluminide A and B coatings failed to protect the blades from corrosion attack. In several regions along the concave side of the leading edge, hot corrosion attack had completely breached the aluminide coating. The corrosion fronts on the aluminide A coated blades and the aluminide B coated blades resembled the finger-like morphology of Type I (HTHC), as distinct from the broad corrosion front of Type II (LTHC). Although the extent of attack on the concave side of these blades was severe, the convex side remained substantially unaffected.

The leading edge of the platinum/rhodium-modified aluminide remained essentially intact with platinum still in plentiful supply on the surface, defined as a bright region in the micrograph at the edge of the coating, thus providing resistance to further attack. However, a small area on the concave side had been penetrated to a depth of about 40% of the original coating thickness. Overall this coating appeared to have provided satisfactory resistance to hot corrosion with further serviceable life remaining.

With all the recent interest in platinum-modified coatings offering superior resistance to hot corrosion over other aluminide coatings it is difficult to explain the excessive attack apparently present on these blades as shown in Figure 4. However, the micrograph shown in

Figure 9(d) presents no evidence of attack. In fact, subsequent sectioning and polishing of this blade showed no sign of hot corrosion at all. The lack of a bright platinum compound, namely $PtAl_2$, on the blade surface provided evidence that it had probably diffused into the solid solution of the surface aluminide. Although this micrograph did not indicate extensive oxide penetration on either the concave or convex sides, there was evidence of the diffusion zone showing signs of depletion. Once the supply of the platinum and chromium is exhausted, this blade will begin to corrode.

Comparing the six micrographs in Figure 9, it was reasonable to conclude that the chromium-modified aluminide offered the least resistance to hot corrosion and oxidation attack. In addition to the excessive attack on the concave side, the convex region had also suffered from moderate hot corrosion. Judging from micrographs only, one would have to rate the platinum and platinum/rhodium modified aluminide leading edges the more superior coatings. Although the silicon-modified aluminide fared well, its rough surface would indicate it to be less effective than the platinum-modified aluminide coatings.

3.2.2 Silicon-modified nickel aluminide coatings

Both silicon-modified coatings represented in Figure 10 indicated severe outward diffusion of aluminium and chromium with some of the molybdenum and tantalum rich precipitate compounds, originally present in the outer zone, all dissolved into the aluminide solid solution. The diffusion zone had almost completely dissolved in most areas of the concave face of Figure 10(a) with coarsening of grains in the coating on the convex face. In contrast, Figure 10(b) indicated that this coating still maintained a diffusion zone that was abundant in the more important elements.

The oxide of the former coating (Figure 10a) consisted primarily of alumina (Al_2O_3) with smaller amounts of silicon, chromium and titanium. The presence of rutile (TiO_2) in the scale is to be expected given it has a very high free energy of formation, higher than that of chromia (Cr_2O_3). While the micrograph showed a lack of a diffusion zone, the qualitative line scans indicated otherwise; several chromium rich areas were apparent. The bright precipitates throughout the coating and substrate were found to be tantalum rich carbides. These bright precipitates were also present in the magnified view, the dark compounds being phosphorous/chromium rich and the grey needle-like compounds being, most probably, the chromium/molybdenum rich sigma phase.

A relatively thick oxide layer in the latter coating (Figure 10b) consisted of, in decreasing order, alumina, chromia and rutile. Other elements present in the oxide were silicon, nickel and phosphorous. The diffusion zone consisted mainly of chromium and titanium (greyish regions) and bright molybdenum and tantalum carbides (MoC, TaC). The remaining β-NiAl region, thinner than its original thickness, suggested that the coating had experienced some form of spallation or excessive oxide formation. The high magnification

micrograph of this coating at the oxide interface indicated that simple oxidation was the major mechanism involved in the attack. The bright layer at the oxide/coating interface of the magnified view was analysed to be niobium rich with the dark β-NiAl grains surrounded by a nickel rich solid solution. The few bright spots on this micrograph were MoC and TaC. Platelets of the hard and brittle sigma phase, whose presence is detrimental to the coating's performance, can be seen in an adjoining area in Figure 16(b).

3.2.3 Nickel aluminide coatings (type A)

It was anticipated that microanalyses of these coatings would reveal extensive regions of degradation. Both blades had indeed suffered from hot corrosion attack but to varying degrees. The macrographs of Figure 2 together with the micrographs of Figure 11 confirm this.

The type of attack, illustrated in Figure 11(a), is manifest as an extensive oxide layer with areas of intense needle-like penetrations into the substrate and occurring along the entire concave leading edge. These needles were found to be aluminium rich oxides. Evidence of a debonded oxide scale, seen as a sharp dip in the line scan, combined with porous areas in the oxide, signify that this blade is on the verge of complete catastrophic degradation. Qualitative results of the oxide scale suggested the outer oxide was predominantly alumina with an underlying oxide, in the vicinity of the advancing oxide front, a mixture of chromia and nickel oxide. The mere fact that nickel oxide was abundant in the oxide scale indicated that the coating was no longer offering any protection. Large bright precipitates were mainly niobium and tantalum rich carbides (NbC, MoC). The magnified micrograph (Figure 11a) shows one of the indicators for hot corrosion attack, namely chromium-sulfide particles, present as small dark specks.

Alternatively, the other Aluminide B coated blade of Figure 11(b), although suffering from moderate oxidation in certain areas, appeared well protected from further attack. It should be noted that the area shown in Figure 11(b) was not representative of the leading edge but from another area that had suffered the maximum degree of attack. On the whole, this coating appeared to be in very good order. The oxide scale, as in the previous blade, consisted mainly of alumina, chromia and nickel oxide. Two types of grains, distinguished by differences in their grey contrast, were evident in the region between the diffusion zone and oxide scale. Both grains were β-NiAl with the lighter shaded grains containing a moderate percentage of chromium. In addition, the complex diffusion zone illustrated a three zone region. The darkest areas were mainly NiAl/chromium compounds; the lighter precipitates were mainly a chromium base containing additions of refractory elements such as molybdenum and tungsten. The brightest areas were tantalum and titanium carbides. Although the magnified view of this coating showed quite extensive oxidation, it was only localised in a small area on the concave face. Minimal amounts of sulfide particles were located.

3.2.4 *Chromium-modified nickel aluminide coatings*

This was the only coating investigated that had experienced severe hot corrosion on both the concave and convex faces. The attack extended deep inside the blade well beyond the diffusion zone. The coating on the concave face of both blades had suffered so badly that the diffusion zone was beyond recognition. A common feature noted in both these micrographs (Figure 12a,b) was the presence of large blocky alumina precipitates below the oxide layer as well as the fine needle-like structure of chromium rich oxides.

The oxide layer of Figure 12(a) consisted of a four zoned structure. The darkest regions, evident mainly as small inclusions, were alumina precipitates. The dark grey areas, abundant as a thick band on the oxide surface and as a narrow band at the oxide/substrate interface, was chromia. Light grey regions, dominant throughout the centre of the oxide layer, were predominantly nickel-rich oxides. Finally, small precipitates of tungsten and tantalum carbides, present as bright 'spots', were identified. Minor additions of phosphorous and sodium were also present in the oxide scale. As in the previous coating, the fact that nickel had begun to readily oxidise suggests that the coating had been depleted of all its aluminium and chromium. This only re-affirms the fact that this coating has been consumed and is no longer protecting the leading edge of the substrate alloy. Grain boundary ingress of alumina is indicated by an arrow at the bottom right corner of Figure 12(a). This proved that the coating had reached a stage where aluminium was no longer available for the formation of a protective oxide scale, but preferential internal oxidation of substrate material was occuring. Grain boundary oxidation can also be observed, together with the presence of chromium-sulfide particles, in the high magnification micrograph.

The microstructure of Figure 12(b), although demonstrating a thinner oxide scale, was very similar to the previous blade. Several large bright tungsten and tantalum rich carbides were evident in the depleted diffusion zone. If readily oxidised, these carbides can have an adverse effect upon resistance to hot corrosion [11]. Thus, it is of prime importance to ensure these refractory elements are restricted in their movement towards the surface otherwise volatile oxides may form. A closer view of the advancing corrosion front provided evidence of sulfur rich particles surrounded by chromia and alumina. The microstructure of this coating can be summarised in the following manner: large blocky precipitates of alumina; small needle-like phases rich in chromia and smaller round particles, in the vicinity of the advancing corrosion front, of chromium sulfides.

3.2.5 *Platinum-modified nickel aluminide coatings*

The platinum-modified aluminide coatings suffered from severe outward diffusion of important elements near the leading edge of the concave face. However, only one coating exhibited significant hot corrosion attack. This was localised in a small area near the middle of the concave face. The other coating showed minimal attack. When these micrographs are compared to the apparently poor performance depicted in the macro-photographs of these

blades in Figure 4 some anomalies are noted. Careful observations of Figure 4(b) at the degraded area interface showed a bright silver-coloured region. This region was very characteristic of a recently spalled area since the underlying alloy had not yet oxidised. It would seem that these blades had suffered from a large degree of spallation of the oxide layer and the outer NiAl phase. From these observations it appears that hot corrosion did not occur to any significant extent.

The outer oxide scale of the partially attacked blade illustrated in Figure 13(a) consisted of the common chromium, aluminium and nickel oxides in addition to small quantities of phosphorus and sodium. The amounts of these latter two elements diminished further toward the oxide/aluminide interface. Closer examination of the oxide in this coating revealed a number of bright specks that were found to be pure platinum metal. The aluminium, originally present in these compounds, may have diffused outwards into the oxide The large bright precipitates adjacent to the diffusion zone were tantalum and niobium carbides ahead of the needle-like sigma phase rich in molybdenum and chromium. This deleterious phase is also shown in greater detail in Figure 16(a). This high magnification image of the corrosion front also depicts small areas of sulfide penetration. However, the surface degradation here is attributed mainly to high temperature oxidation.

The second blade illustrated in Figure 13(b) had experienced even less attack than the previous blade. Qualitative analyses revealed a platinum rich phase, most probably $PtAl_2$, at the oxide interface represented by a bright area; a sufficient aluminium reservoir to prevent unfavourable oxidation of substrate elements; a chromium rich diffusion zone and a thin oxide layer. Once again the large bright tantalum carbide particles were present, surrounded by large blocky chromium/molybdenum rich phases and darkish phosphate precipitates. Phosphate rich regions may originate from the processing methods used in applying these coatings. The high proportion of β-NiAl retained in this coating indicates a capability to provide further continued oxidation/corrosion protection. A magnified view of the diffusion zone illustrated four distinct phases: (i) a dark phase rich in chromium and phosphorus; (ii) a light grey phase that consisted mainly of chromium and a small amount of molybdenum; (iii) the bright tantalum and tungsten carbides and finally (iv) the needle-like sigma phase rich in molybdenum, chromium and nickel.

3.2.6 Platinum/Rhodium modified nickel aluminide coating

The role of rhodium in this coating, detected in both the scale and outer coating, was to provide added oxide adherence thus, reducing the tendency of spallation. Although Figure 9(e) illustrates that the leading edge of this coated blade had oxidised somewhat, it was only localised in a small area near the tip. In all other aspects, this micrograph of Figure 14(a) appeared almost identical to the micrograph of the platinum modified aluminide in Figure 13(b). The oxide consisted almost entirely of alumina and chromia with evidence of platinum present. At the coating/oxide interface two phases were apparent. A greyish region, found to

be rich in chromium, followed by a brighter dispersed area more abundant in platinum and rhodium. The greyish phase is chromia on the verge of forming a protective scale. The brighter area probably contained an array of compounds ranging from $PtAl_2$, Pt_2Al_3 and (Ni,Pt)Al. Phosphate rich phases, present as dark phases in the diffusion zone, owe their existence to chemicals used in processing this coating. The lighter regions in the diffusion zone were chromium/molybdenum rich phases. The absence of any advancing chromium-sulfide front in the magnified view of this coating indicated that Type I (HTHC) was absent. Simple oxidation seemed to be the only mode of attack on this coating. The high-magnification micrograph revealed a microstructure almost identical to the previous blade. The dark phases consisted of chromium/phosphorous with the grey regions, most likely the sigma phase, being abundant in chromium/molybdenum.

3.2.7 Nickel aluminide coating (type B)

Extensive attack was evident along most of the concave face often reaching to the substrate. A typical microstructure of an area near the leading edge on the concave face is shown in Figure 14(b) indicating severe oxidation and hot corrosion. Finger-like penetrations on the right side of the micrograph are typical of Type I (HTHC). The oxide was predominantly alumina near the surface with chromia more abundant further in towards the oxide/coating interface. X-ray linescans also suggest that nickel oxide was present. Likewise, porosity of the oxide was evident. In the diffusion zone bright tantalum and tungsten carbides were noted; greyish chromium/molybdenum rich precipitates and the darkish α-chromium phase. A close analysis of the corrosion front indicated the presence of chromium sulfides represented as small dark circular spots.

4. DISCUSSIONS

It has been well documented that if HPT blades are to provide extended service lives, they rely on the integrity of the protective oxide scales, such as alumina and chromia, formed on their surface. However, these two oxides each have their shortcomings. The chromia scale will not form if the chromium content falls below 10-15%. Furthermore, at elevated temperatures chromia will be oxidised to form CrO_3, a volatile gaseous species. Recent estimates conclude that the maximum temperature at which these alloys can be used is somewhat less than 850°C [9]. These T56-HPT blades would very likely have experienced temperatures in excess of 900°C. This may explain the poor results of the chromium-modified aluminides. Although alumina scales generally do not oxidise further to volatile species and are thermodynamically more favoured to form than chromia, they grow at a significantly slower rate than chromia scales.

It has been shown that macroscopic evaluations of blade coating performance must be coupled with microscopic observations if meaningful results are to be obtained. For instance,

the silicon-modified aluminide appeared unbreached to the naked eye but in fact had been almost completely consumed when microscopically examined. In contrast, one of the platinum-modified aluminide coatings that appeared severely attacked from the macrograph of Figure 4(a) was found to be more than satisfactory when observed through the microscope. Microscopic examination revealed that the attack was only superficial spallation of the oxide scale and that sufficient aluminide coating remained to protect the underlying turbine blade material.

The results obtained within this report enabled a table to be constructed, Table 3, which ranks the ten coated blades in terms of their hot corrosion, oxidation and spallation resistance. The table confirms the notion that platinum-modified aluminides offer superior resistance to degradation than other conventional and modified aluminides. Platinum is known to improve the corrosion resistance of the coating by increasing the activity of the aluminium in the coating enabling a very protective and adherent alumina scale to form on the surface [10]. It acts as a diffusion medium which allows aluminium to establish a nickel aluminide sub-surface and, simultaneously generate a platinum-aluminium intermetallic skin [11]. In contrast, the conventional aluminide coatings A and B rely solely on the formation of alumina and chromia to protect the blade material and prevent hot corrosion.

To explain the reasons why one coating was more resistant to attack than another coating, one must appreciate that most hot corrosion processes can be divided into incubation, initiation and propagation stages. The duration of the incubation and initiation stages is dictated by a number of factors including alloy and coating composition, temperature fluctuations and gas velocity, to mention only a few. Thus, the basic nickel aluminides and chromium-modified aluminides, on all accounts, may have shorter incubation and/or initiation stages than the platinum-modified aluminides. Varied results can also be obtained from similarly coated blades. This is evident from the conflicting results of the two aluminide A coatings. The variables, inlet air velocity, foreign object damage and erosion, can seriously influence the performance of a particular blade. One set of coatings that experienced consistent though poor results were the chromium-modified aluminides suggesting a relatively easy incubation and initiation of hot corrosion with these coatings.

There was no evidence in the microstructure of any of the aluminide coatings that they had experienced the more severe Type II (LTHC) which is characterised by a pitting attack, with little or no internal sulfidation or alloy depletion. Nevertheless, there were extensive areas of Type I HTHC, characterised by a broad corrosion front with internal chromium-rich sulfides and a layer, within the alloy, depleted in the more reactive elements. This re-affirms the fact that the blades had generally faced temperatures greater than 750^{o}C, the maximum temperature where Type II LTHC occurs. High temperature oxidation, consistent with temperatures above about 900^{o}C, were observed.

The mechanisms of hot corrosion (sulfidation) of alloys are similar to those of oxidation processes. However, sulfidation is up to five orders of magnitude faster than oxidation. In addition the metal sulfide or metal/metal sulfide eutectics usually have low melting points. The presence of sulphur deep within the coating may be explained by the 'sulfidation-oxidation' model, first proposed by Simons [12] and later modified by Spengler [13]. The deposition of sulfates, namely Na_2SO_4 and $CaSO_4$, on the turbine blade surface causes the sulfur to diffuse into the alloy to form Cr_3S_4 particles, which are oxidised, releasing free sulfur. The sulfur diffuses inward and new Cr_3S_4 is formed again:

$$2Cr_3S_4 + 9O \rightarrow 3Cr_2O_3 + 8S$$

$$8S + 6Cr \rightarrow 2Cr_3S_4$$

Thus, the sulfur advances gradually and this process is self-sustaining. It must be understood that this is only one of many models proposed since the first recognition of hot corrosion in 1950. Different mechanisms may be operative depending on alloy composition, temperature range etc.

The loss of aluminium and chromium due to spallation allowed other oxides, more likely to offer inferior hot corrosion resistance, to form at increased rates. This leads to rapid coating failure. The first sign of nickel oxide formation in the oxide scales implies a deficiency of available aluminium and chromium and failure of the aluminide coating. As a result, the production of the protective alumina and chromia scales are halted. High concentrations of nickel oxide in the chromium-modified aluminide are visible in Figure 12(a) and its respective line scans. In contrast, Figure 14(a) presents a dark oxide scale deficient in nickel and abundant in aluminium and chromium.

In general, nickel based superalloys contain three major types of carbides: MC, $M_{23}C_6$ and M_6C (M=metal). A fourth type, M_7C_6 is seldom seen and usually transforms to $M_{23}C_6$ at elevated temperatures. The M_6C carbide only forms in alloys when the chromium to molybdenum plus tungsten content (Cr/(Mo+0.4W) is less than 3.7 [14]. Hence, the dominant carbides in this alloy would appear to be the MC and $M_{23}C_6$ phases. The blocky morphology of the extremely stable MC carbide distinguishes it from the elongated nature of the $M_{23}C_6$ compound present mostly along grain boundaries. Whereas the former carbide consists of refractory rich phases such as (TaC, NbC, MoC, WC etc.), the latter carbide mainly forms $Cr_{23}C_6$. Very small amounts of zirconium and boron in the alloy, as indicated in Appendix I, greatly improve the mechanical properties of the grain boundaries by means of promoting impurity segregation [9].

The occurrence of the hard and brittle sigma phase in the diffusion zone of several coating microstructures, including the platinum-modified aluminides, can have adverse effects

on turbine blade performance. This phase tends to decrease or seriously effect the impact strength, creep strength, rupture life and creep ductility of many engineering materials. Additionally, its extensive plate-like morphology introduces an avenue for crack propagation into the matrix. In 1964, Wlodek [15] first positively identified this sigma phase in nickel-based superalloys and characterised the phase as being rich in chromium, molybdenum, nickel and cobalt. The very high concentrations of the solid-solution strengtheners chromium and molybdenum, which are sapped up from the matrix when an aluminide coating fails, considerably weakens the alloy.

The reason for an abundance of phosphate compounds in the diffusion zones of the platinum and platinum/rhodium-modified aluminides is believed to result from processes used for depositing the platinum. Although the majority of coating procedures are proprietary, it is widely known that the electroplating of platinum involves phosphate based compounds such as sodium phosphate ($Na_2HPO_4.7H_2O$) and ammonium phosphate $(NH_4)_2HPO_4$. This appears to be the main cause for the presence of phosphorous in these areas [16]. However, the presence of phosphorous on the coating surface may also be caused by phosphate containing lubricity agents (Table 2) used as a fuel additive.

The need for protective coatings on the surfaces of internal cooling channels of a turbine blade introduces controversy relating to the importance of preferential oxide attack on blade strength and life. The micrograph, Figure 15, gives a clear indication that this is of utmost importance. Severe oxidation and hot corrosion to a depth of up to 60μm is evident in this micrograph.

It appeared that turbine operation (base load versus cycling) can promote spallation of the oxide scale from a range of coatings. Hence, cyclic oxidation can have a profound effect on the performance of various coatings. These effects must be taken into consideration when selecting a coating/substrate system. Details regarding the original conditions of the coatings, processes adopted to deposit the coatings, quality control procedures implemented and the operative history of the turbines were not known. Under these circumstances, combined with the fact that the results should be recognised as limited in scope, the conclusions presented in this report should not be too widely generalised.

5. CONCLUSIONS

The following conclusions can be drawn from the results obtained in this report coupled with relevant information acquired through other sources:

(i) No coating in this report could be described as totally resistant, since even the most protective coating had degraded in localised areas.

(ii) A synergistic effect involving mechanical and chemical processes seems to be the main cause of the high levels of degradation of these gas turbine blade coatings.

(iii) After 2000 hours of engine operation, the condition of the first stage high-pressure blades with the six different coatings ranked from best to worst was platinum/rhodium-modified aluminide >platinum-modified aluminide >silicon-modified aluminide >conventional nickel aluminide (Type A) >conventional nickel aluminide (Type B) >chromium-modified aluminide. Thus, the precious metal aluminides offer the best protection.

(iv) Owing to the high temperatures these blades appear to have faced (850°-900°C) and the morphology of the corroded areas, Type I HTHC was the dominant mechanism. This involves a combined effect of accelerated oxidation and the sulfidation of chromium at the corrosion fronts.

(v) The anomalies which arose when comparing the macrographs and the micrographs of the platinum-modified aluminides confirms the importance of micro-structural and microanalysis. Visual inspection alone can give misleading assessment of coating performance.

(vi) The onset of the formation of the deleterious sigma phase in a majority of the coatings, including the platinum-modified aluminides, is a matter for concern.

6. RECOMMENDATIONS

Platinum-modified coatings should provide superior corrosion resistance to the turbine blades fitted on the RAAF T-56 engines. Protection methods in the following areas are also suggested :

- ensuring the inlet air-stream is well filtered from impurities to obviate hot corrosion as well as minimising compressor fouling;
- using high quality, low contaminant fuels;
- monitoring the amount of ingested alkali salts from sea salt;
- frequent removal of deposits from the blades;
- and the use of fuel additives.

These recommendations should be confirmed with the release of the next set of results from the same T56 engine after having experienced approximately 2500 hours of engine use. This report will be published shortly.

7. ACKNOWLEDGMENTS

The metallurgical preparation side of this report was carried out by Mr. P Rohan and the author. The author would also like to thank Dr. G. McAdam and Mr. J. Shenton for their invaluable advice and discussions. This work was supported by the R.A.A.F., Task No. 88/025, managed by Dr. Neil Ryan.

7. REFERENCES

1 Cocking J.L., Richards P.G. and Johnston G.R., 'Comparative Durability of Six Coating Systems on First Stage Turbine Blades', *Surface & Coating Technol.*, **36**, 37, (March 1988).

2 Russo S.G., 'Field Evaluation of Six Protective Coatings applied to T56 Turbine Blades after 1500 hours of engine use', ARL Report No. ARL-MAT-TM-405, (June 1991).

3 Johnston G.R. and Richards P.G., 'High Temperature Corrosion in Military Gas Turbines: An Initial Metallographic Comparison of the Durability of Two Protective Coatings for First Stage Turbine Blades in TF30-P-3 Engines', MRL Report No. MRL-R-820 (Restricted), (May 1981).

4 Richards P.G., Cocking J.L. and Johnston G.R., 'High Temperature Corrosion in Military Gas Turbines: An Intermediate (754hours) Metallographic Comparison of the Durability of Two Protective Coatings for First Stage Turbine Blades in TF30-P-3 Engines', MRL Report No. MRL-R-909 (Restricted), (Dec. 1983).

5 Richards P.G., Cocking J.L. and Johnston G.R., 'High Temperature Corrosion in Military Gas Turbines: A Final (1029hours) Metallographic Comparison of the Durability of Two Protective Coatings for First Stage Turbine Blades in TF30-P-3 Engines', MRL Report No. MRL-R-992 (Restricted), (April 1986).

6 Cocking J.L., Burley N.A. and Johnston G.R., 'The Degradation of Aluminide Coated First Stage Turbine Blades in the Engines of a Light Military Helicopter', *High Temp. Technol.*, **4**, No. 4, 175, (Nov. 1986).

7 Smialek J.L., 'Adherent Al_2O_3 Scales Formed on Undoped NiCrAl Alloys', *Met. Trans.A*, **18A**, 164, (Jan. 1987).

8 Nicoll A.R., Hildebrandt U.W. and Wahl G., 'The Properties of a Chemical Vapour-Deposited Silicon Base Coating for Gas Turbine Blading', *Thin Solid Films*, **64**, 321, (April 1979).

9 Stringer J., 'High Temperature corrosion of superalloys', *Mater. Sci. & Technol.*, **3**, 482, (July 1987).

10 McMinn A., Viswanathan R. and Knauf C.L., 'Field evaluation of gas turbine protective coatings', *J. of Engin. for Gas Turbines & Power*, **110**, 142, (Jan. 1988).

11 Wing R.G. and McGill I.R., 'The protection of Gas Turbine blades: A Platinum Aluminide Diffusion Coating', *Platinum Metals Review*, **25**. No. 3, 94, (Oct. 1981).

12 Simons E.L., Browing G.V. and Liebhafsky H.A., 'Sodium Sulfate in Gas Turbines', *Corrosion*, **11**, 505, (1955).

13 Spengler C.J. and Viswanathan R., 'Effect of Sequential Sulfidation and Oxidation on the Propagation of Sulfur in an 85Ni-15Cr Alloy', *Met. Trans.*, **3**, 161, (Jan. 1972).

14 Bettridge W. and Heslop J., 'The Nimonic Alloys', 2nd edition, Chapter 4, 50, Edward Arnold Pub. (London), (1974).

15 Wlodek S.T., 'The Structure of IN-100', *Trans. Am. Soc. Met.*, **57**, 110, (March 1964).

16 Gray A.G., 'Modern Elecroplating', Chapter 14, 357, John Wiley and Sons Pub. (New York), (1953).

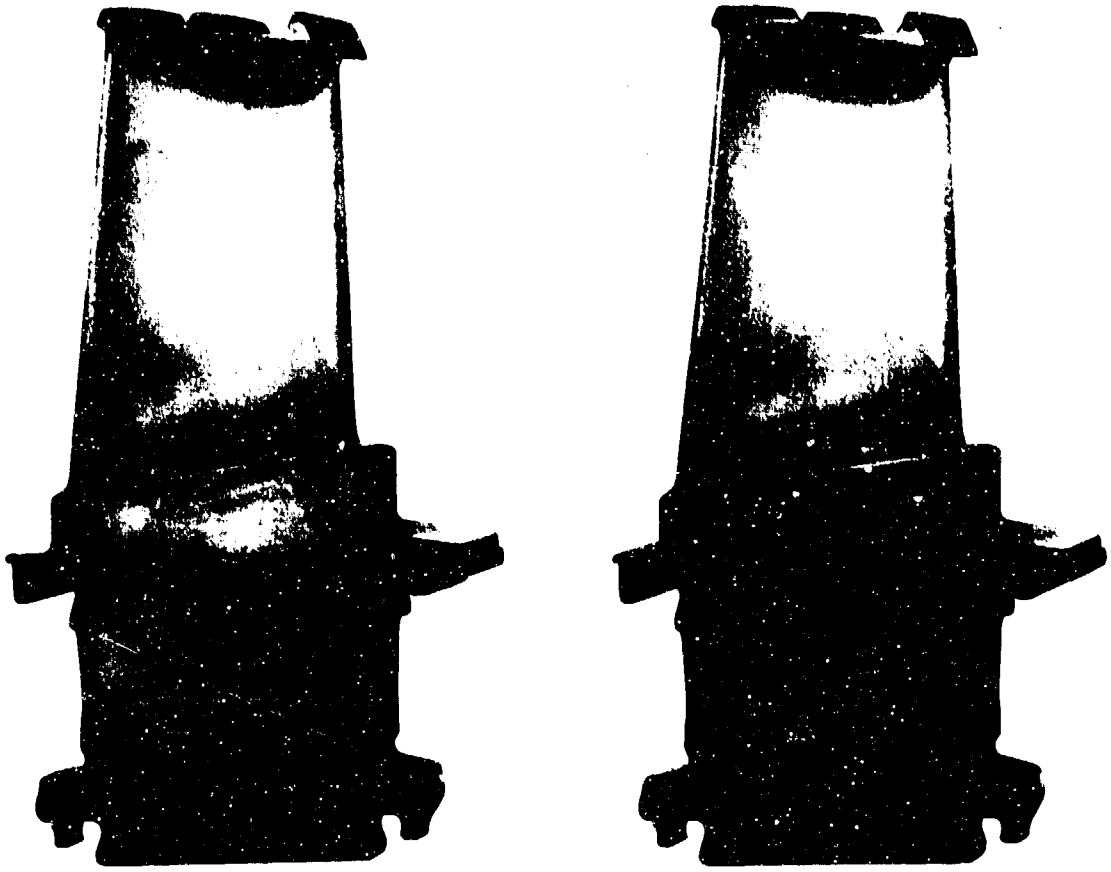

(a) (b)

Figure 1 Silicon-modified aluminide coated blades.

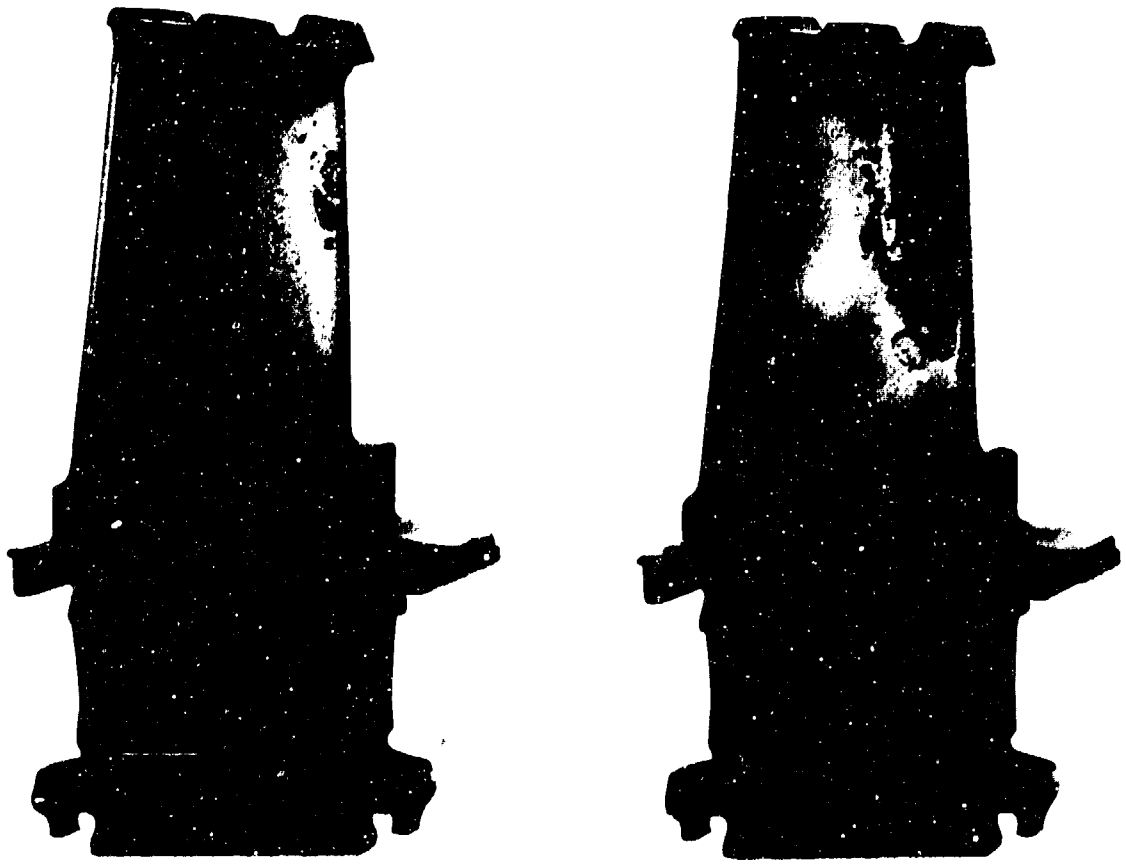

(a) (b)

Figure 2 Conventional nickel aluminide (Type A) coated blades.

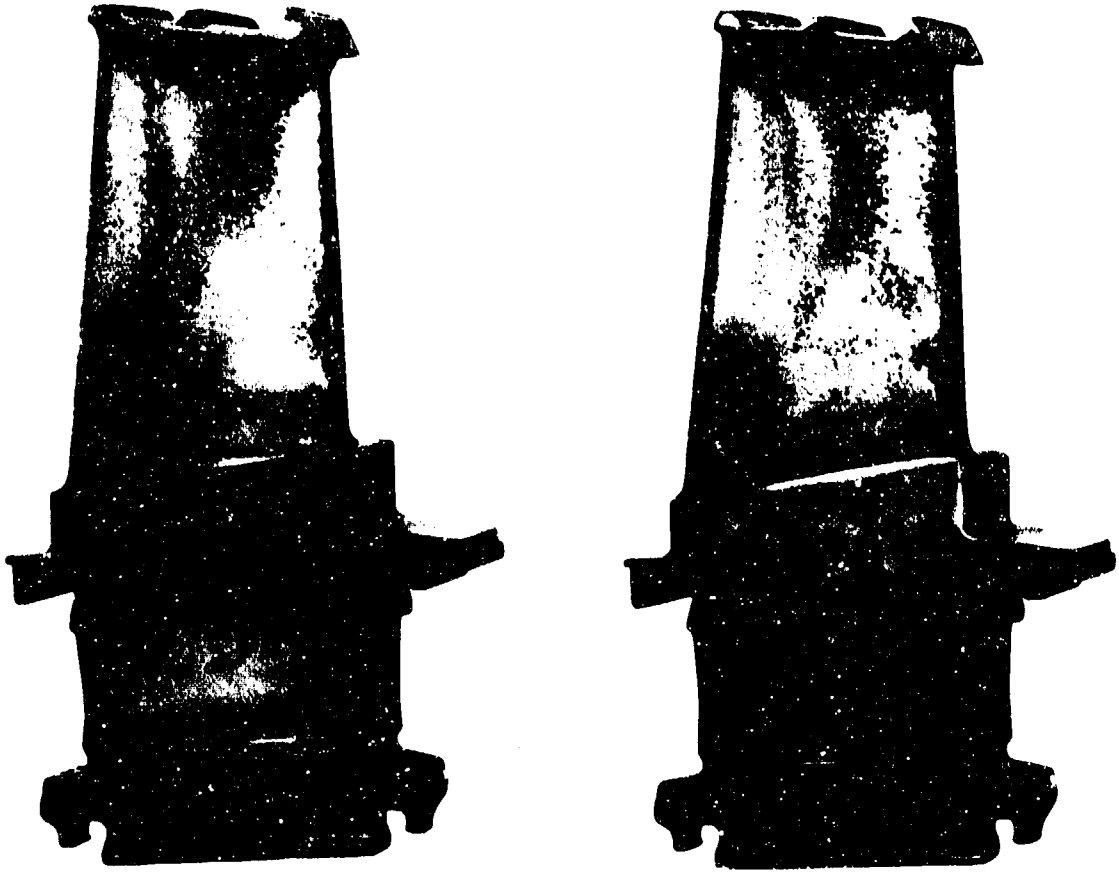

(a) (b)

Figure 3 Chromium-modified aluminide coated blades.

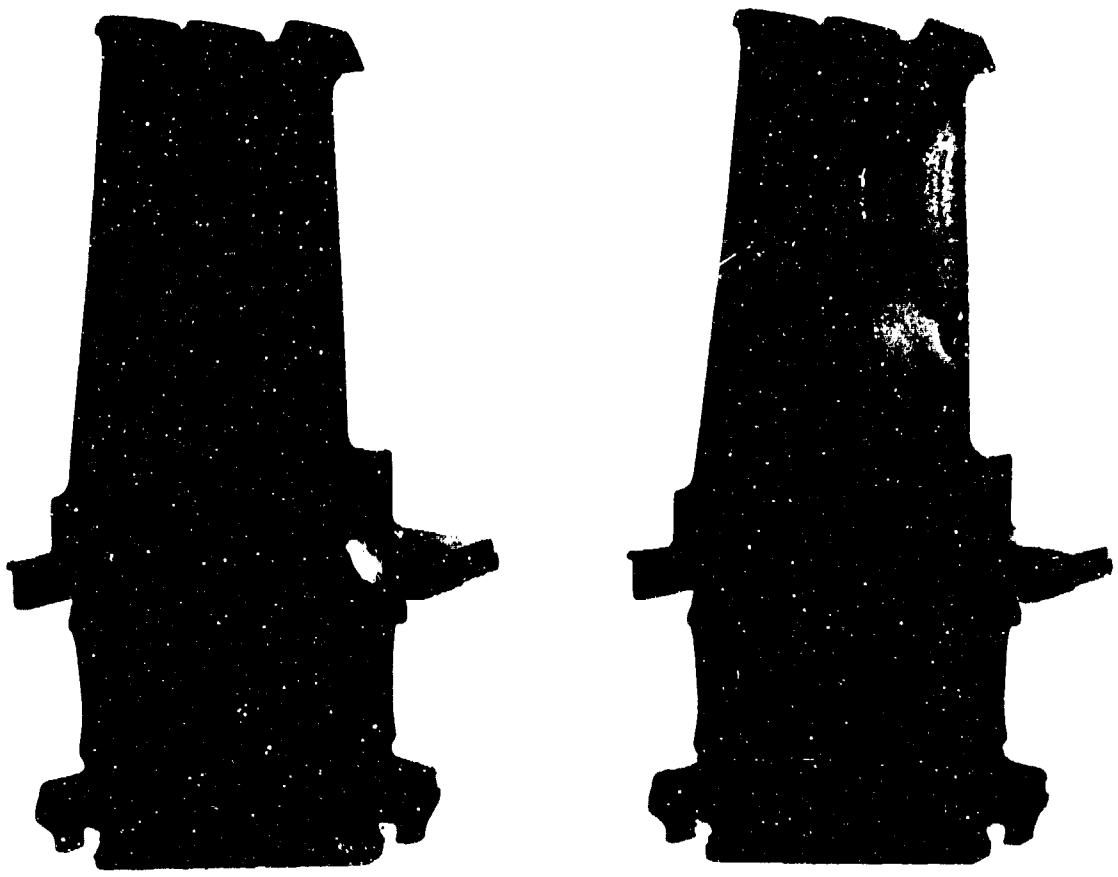

(a) (b)

Figure 4 Platinum-modified aluminide coated blades.

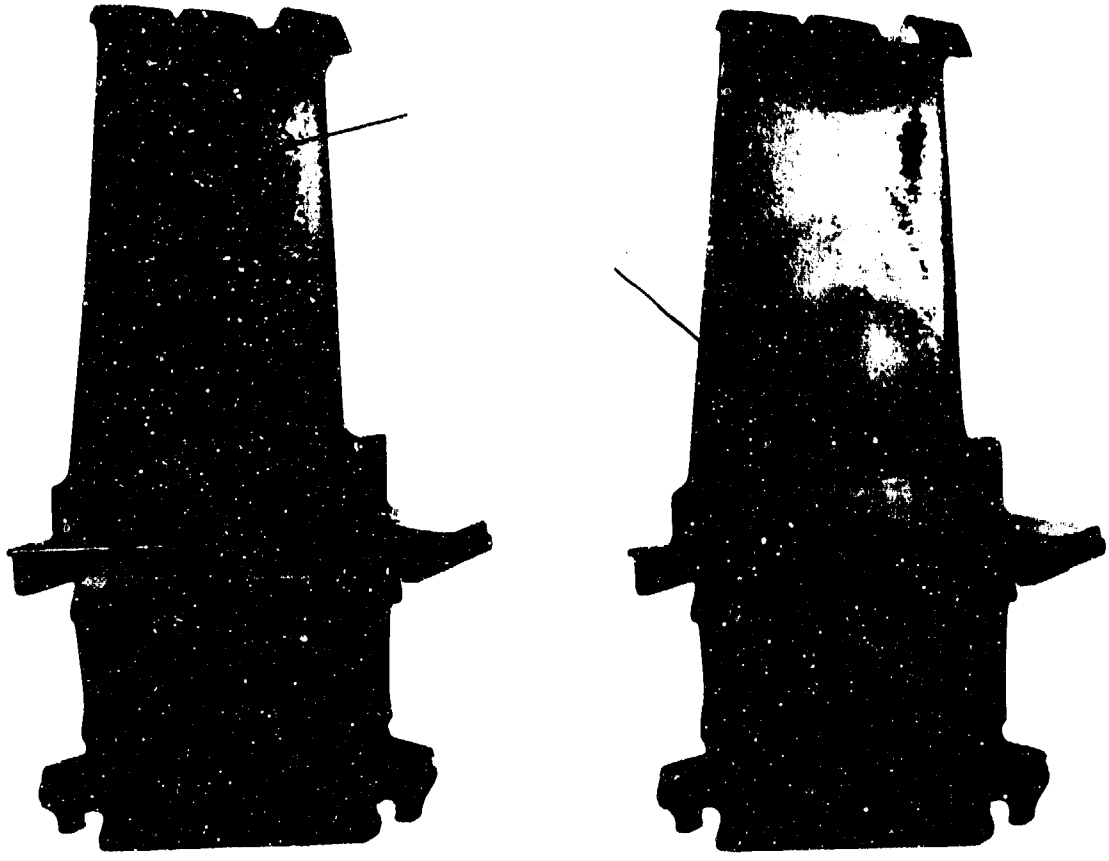

(a) (b)

Figure 5 Platinum/rhodium-modified aluminide coated blades.

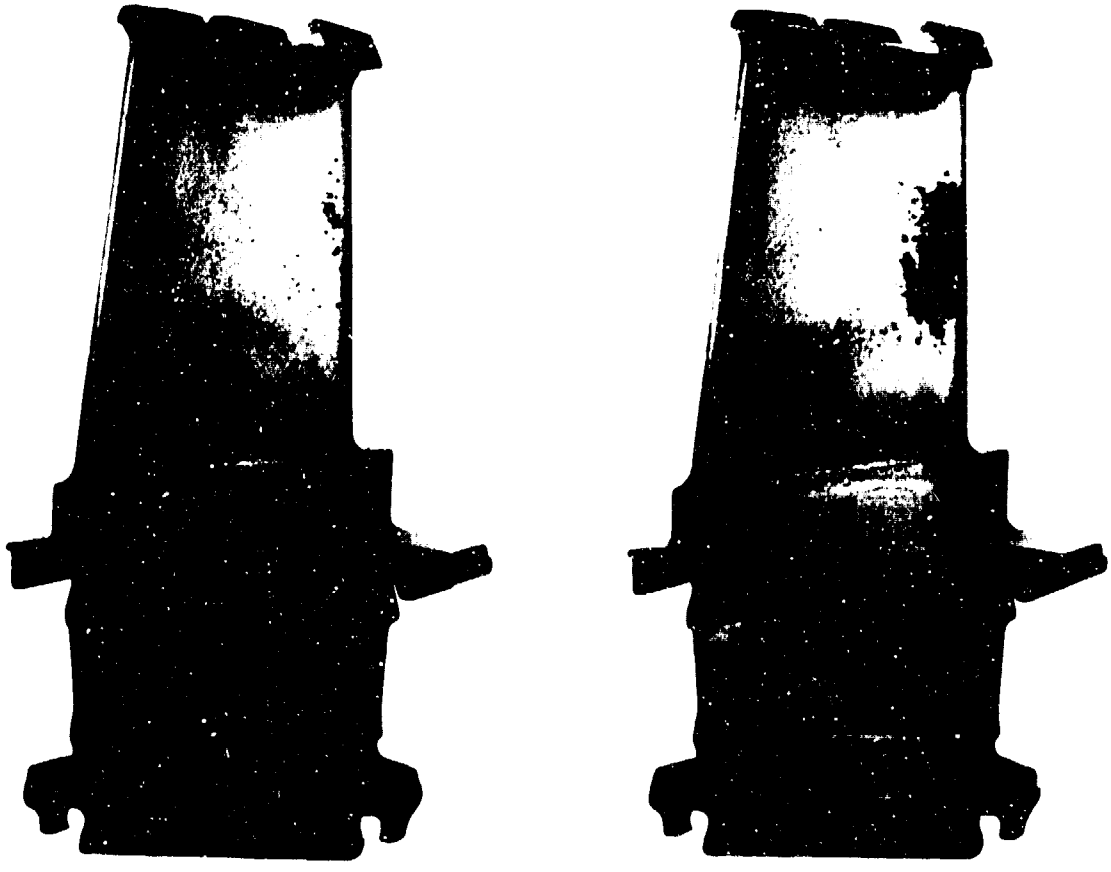

(a) (b)

Figure 6 Conventional nickel aluminide (Type B) coated blades.

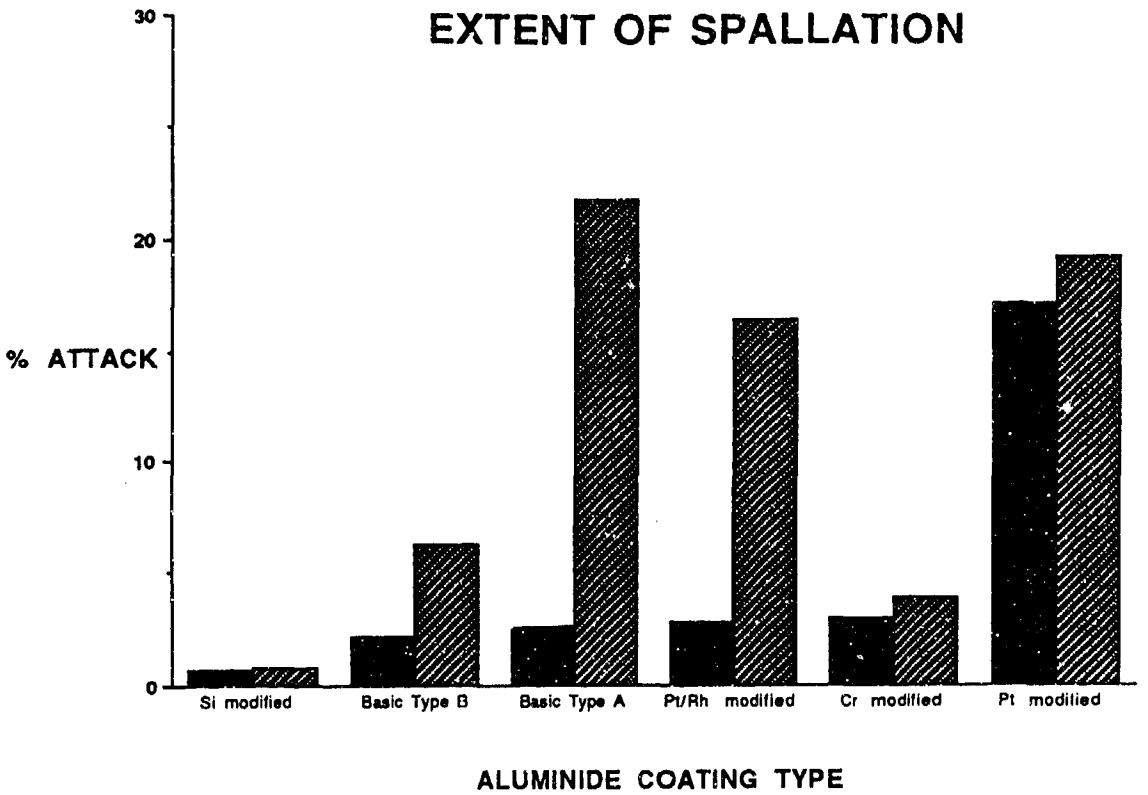

Figure 7 Spallation chart of the concave side of the twelve turbine blades. These results were obtained through macroscopic evaluation.

(i) microscopic analyses indicated these blades had suffered from superficial spallation of the oxide scale with minimal ingression into the substrate

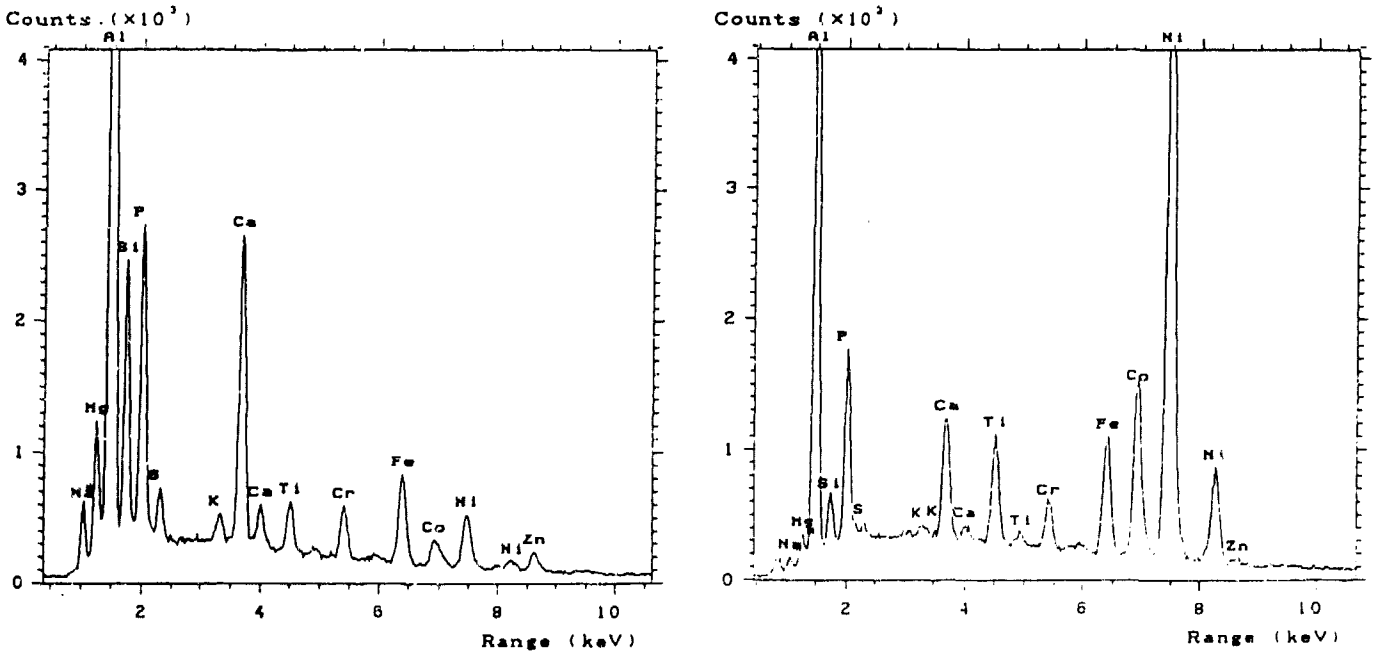

(a) Unattacked region (b) Attacked region

Figure 8 Typical X-Ray spectra of (a) an unattacked and (b) an attacked region from one of the sample turbine blades.

(a) Silicon-modified aluminide.

(b) Nickel aluminide (Type A)

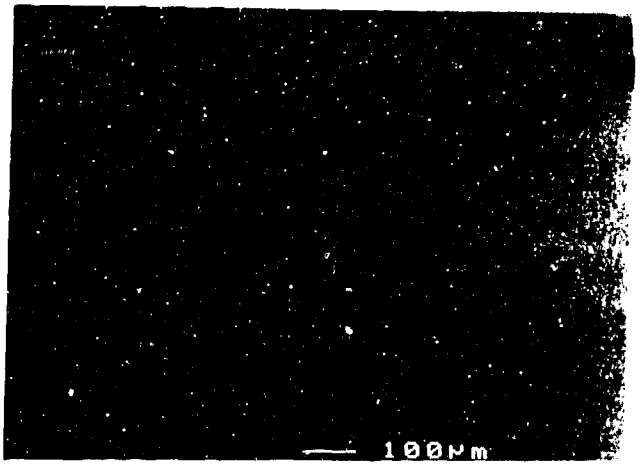

(c) Chromium-modified aluminide.

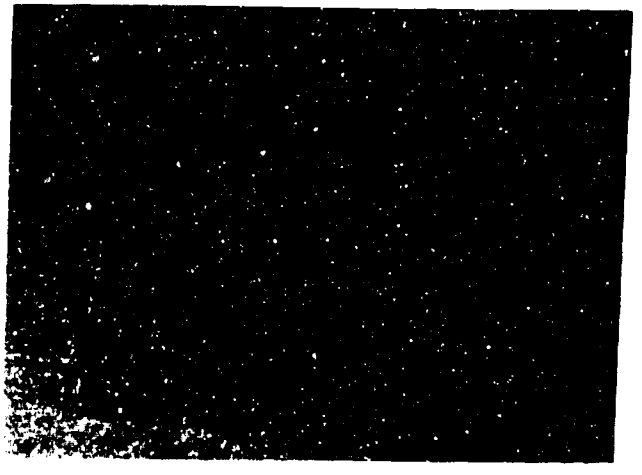

(d) Platinum-modified aluminide.

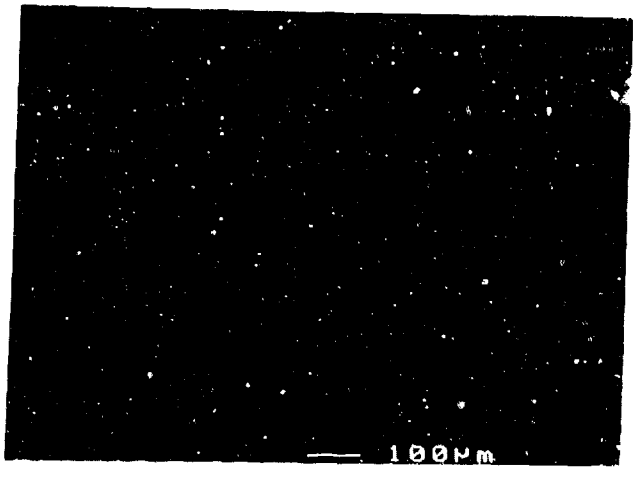

(e) Platinum/rhodium-modified aluminide.

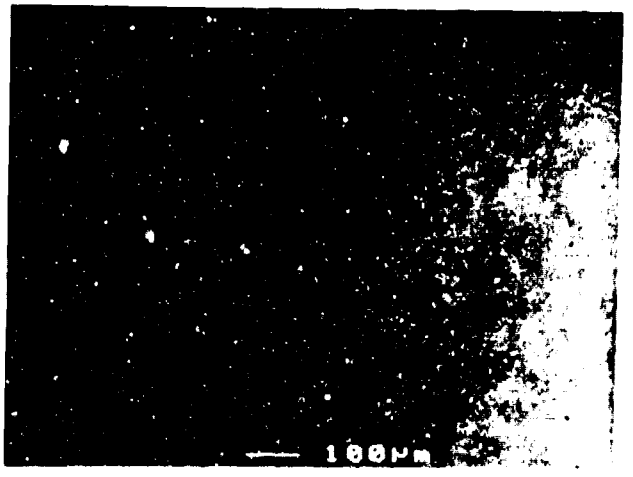

(f) Nickel aluminide (Type B)

Figure 9 Respective micrographs of the leading edges at locations midway between the root platform and shroud tip.

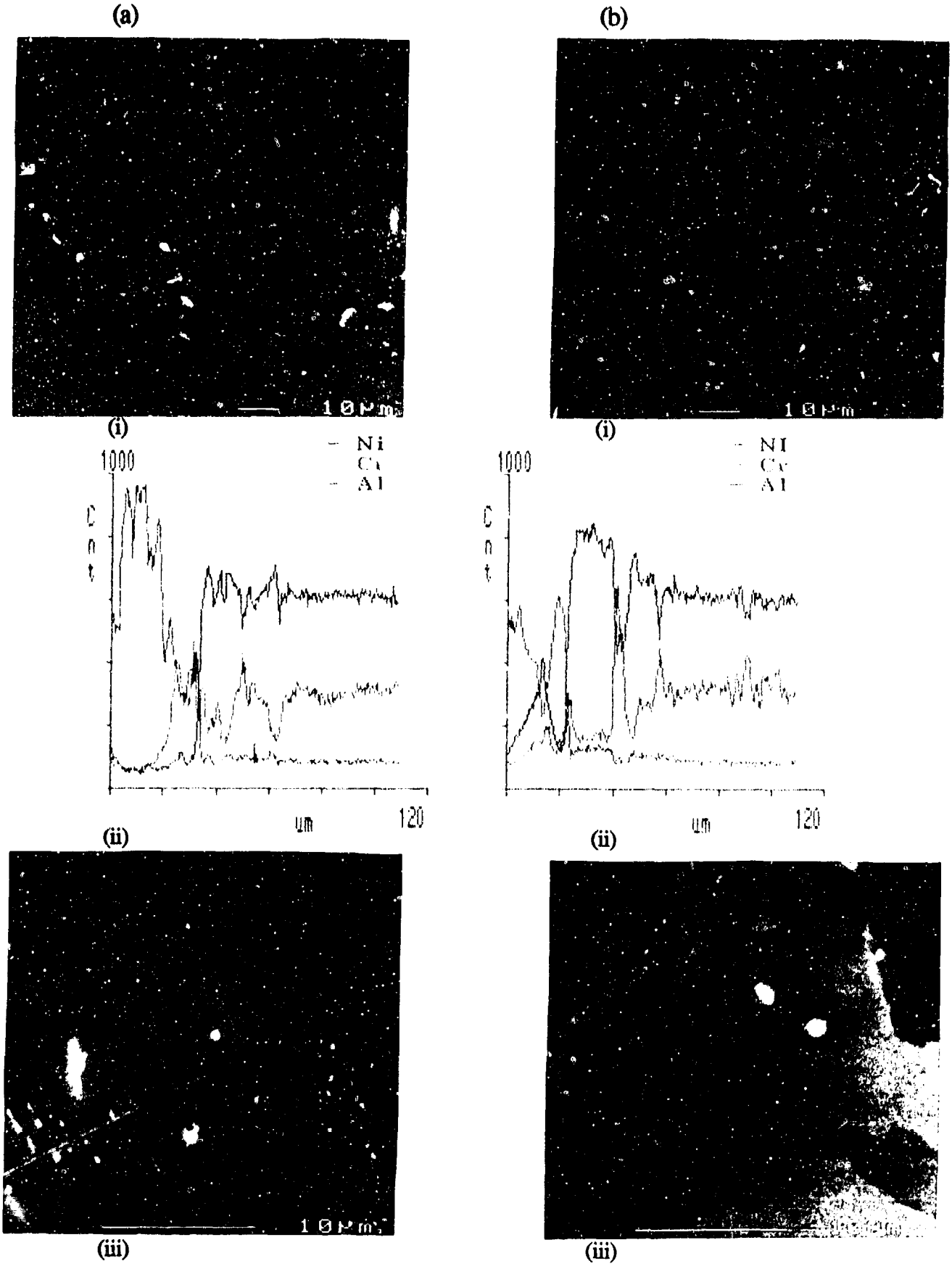

Figure 10 Silicon-modified nickel aluminides (a) and (b) represented as micrographs at the concave leading edges (i) with corresponding line-scans (ii) and a magnified view of the corrosion front (iii).

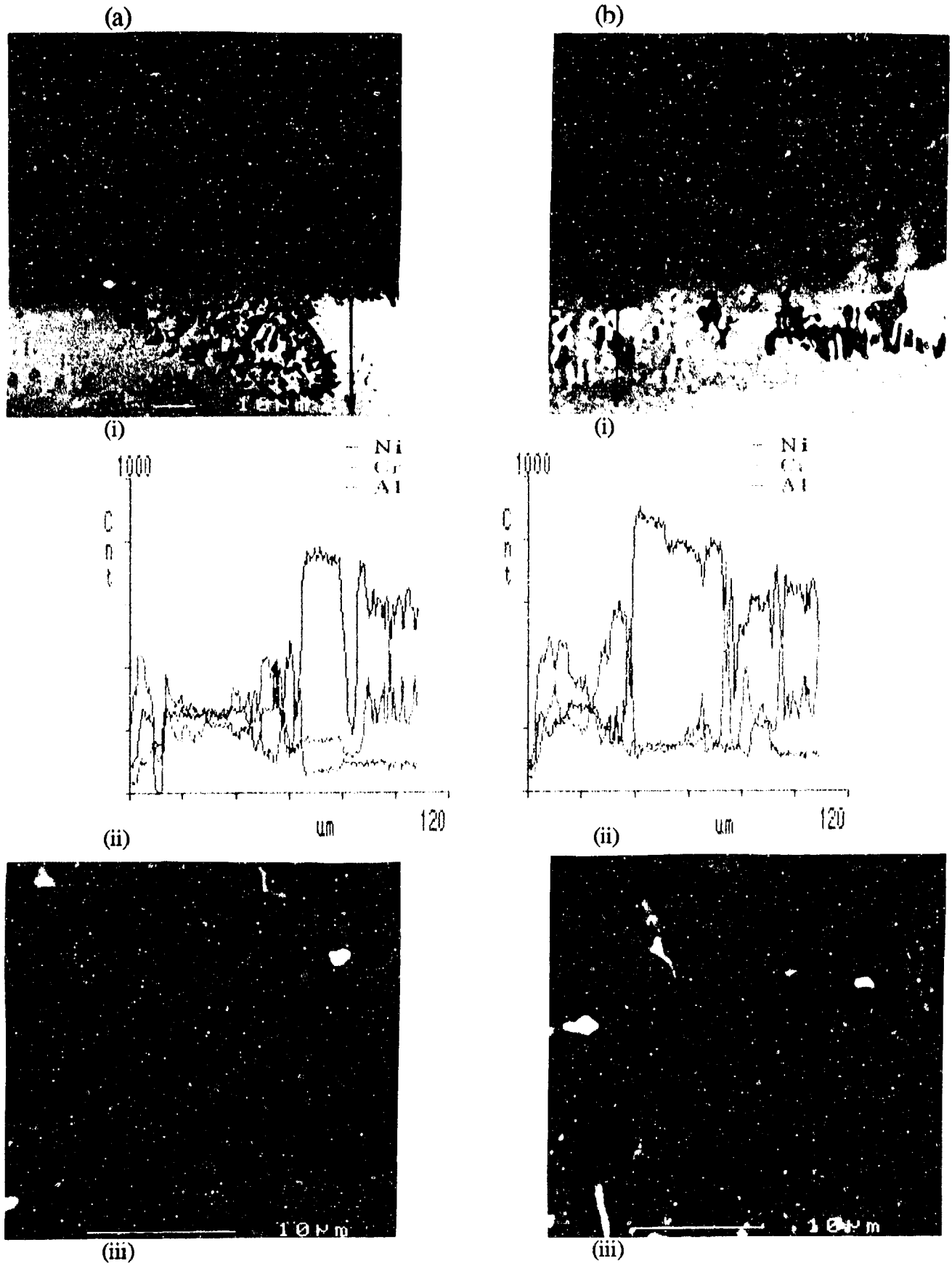

Figure 11 Basic nickel aluminides {Type A} - (a) and (b) represented as micrographs at the concave leading edges (i) with coresponding line-scans (ii) and a magnified view of the corrosion front (iii).

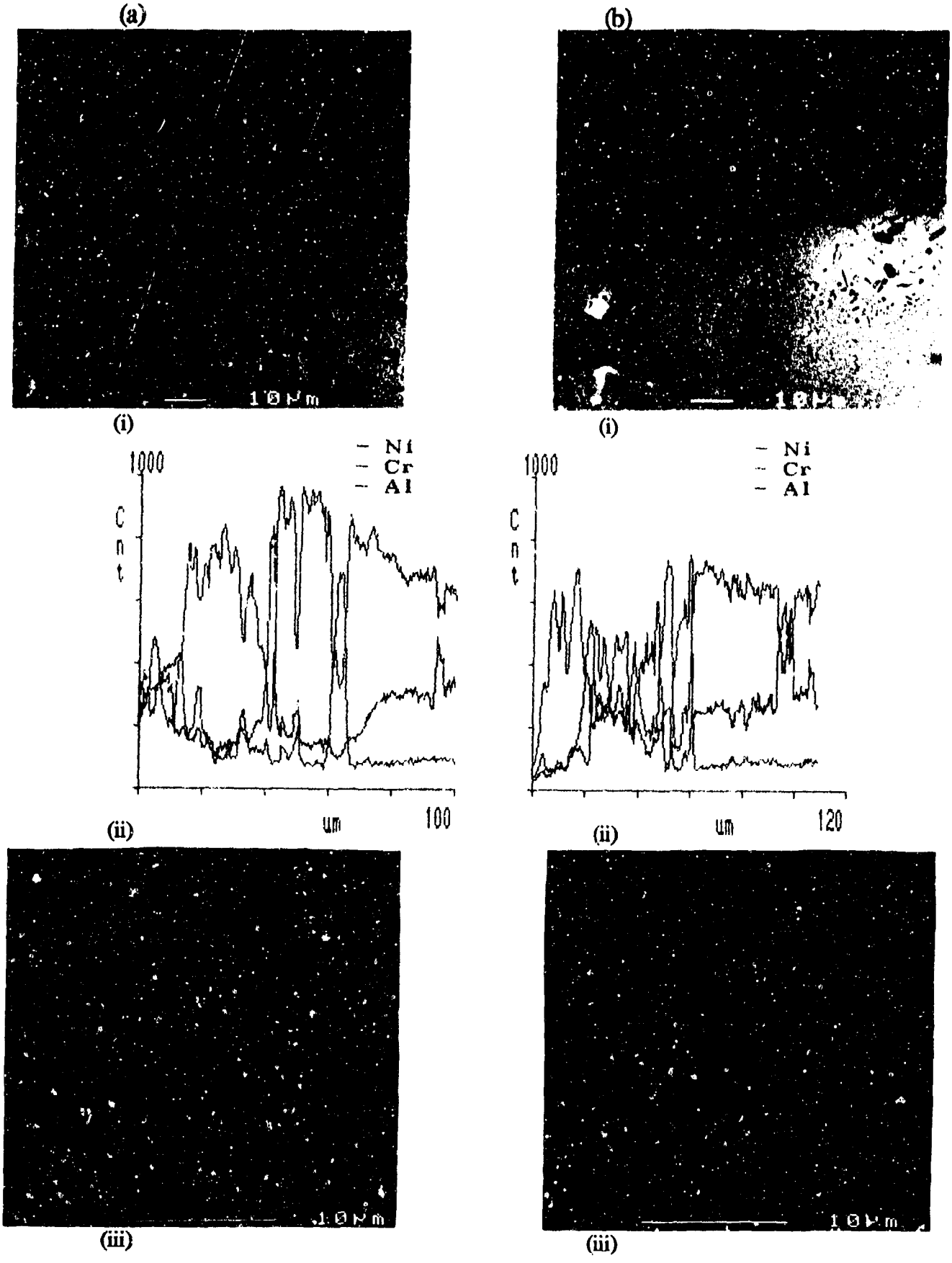

Figure 12 Chromium-modified nickel aluminides (a) and (b) represented as micrographs at the concave leading edges (i) with corresponding line-scans (ii) and a magnified view of the corrosion front (iii).

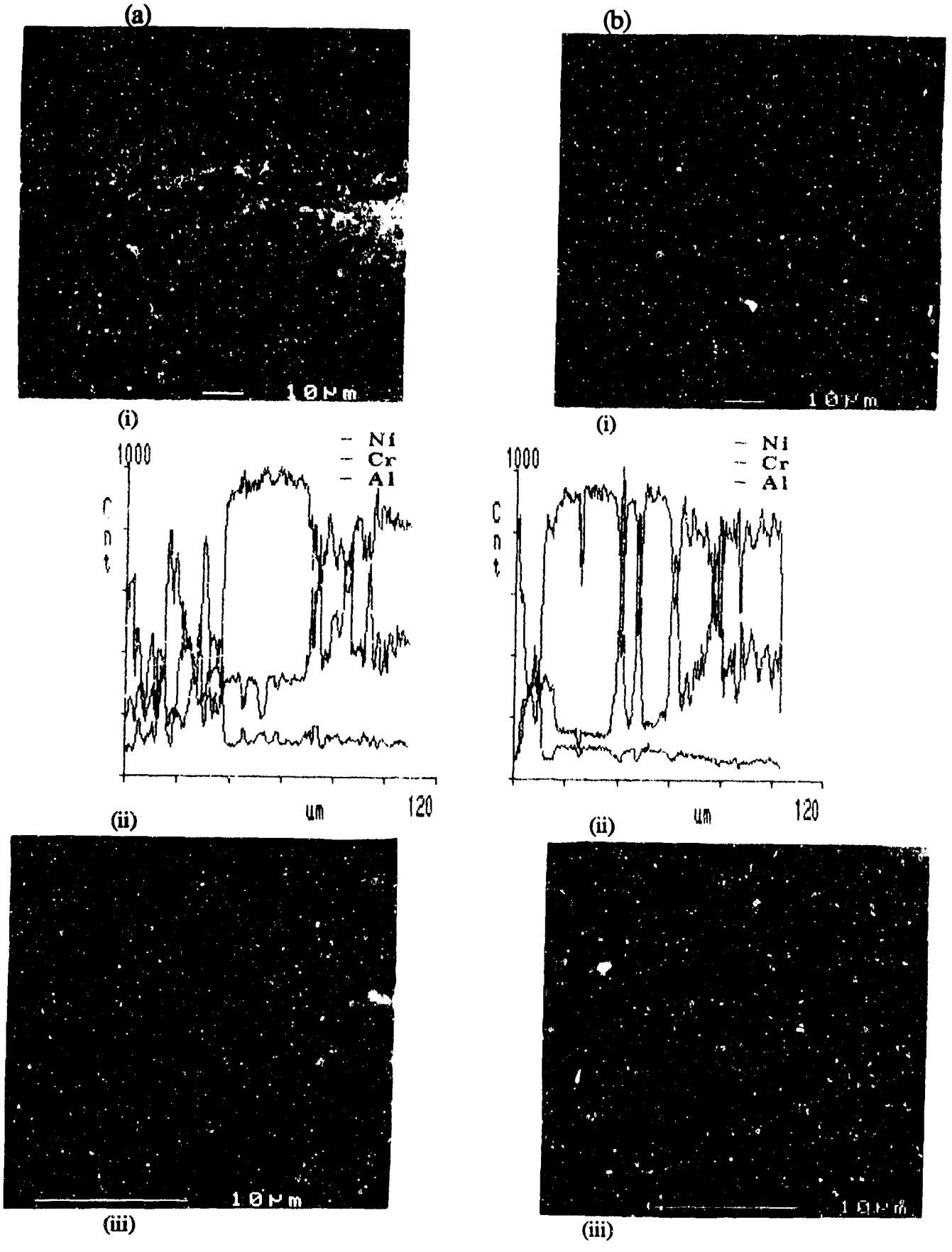

Figure 13 Platinum-modified nickel aluminides (a) and (b) represented as micrographs at the concave leading edges (i) with corresponding line-scans (ii) and a magnified view of the corrosion front (iii).

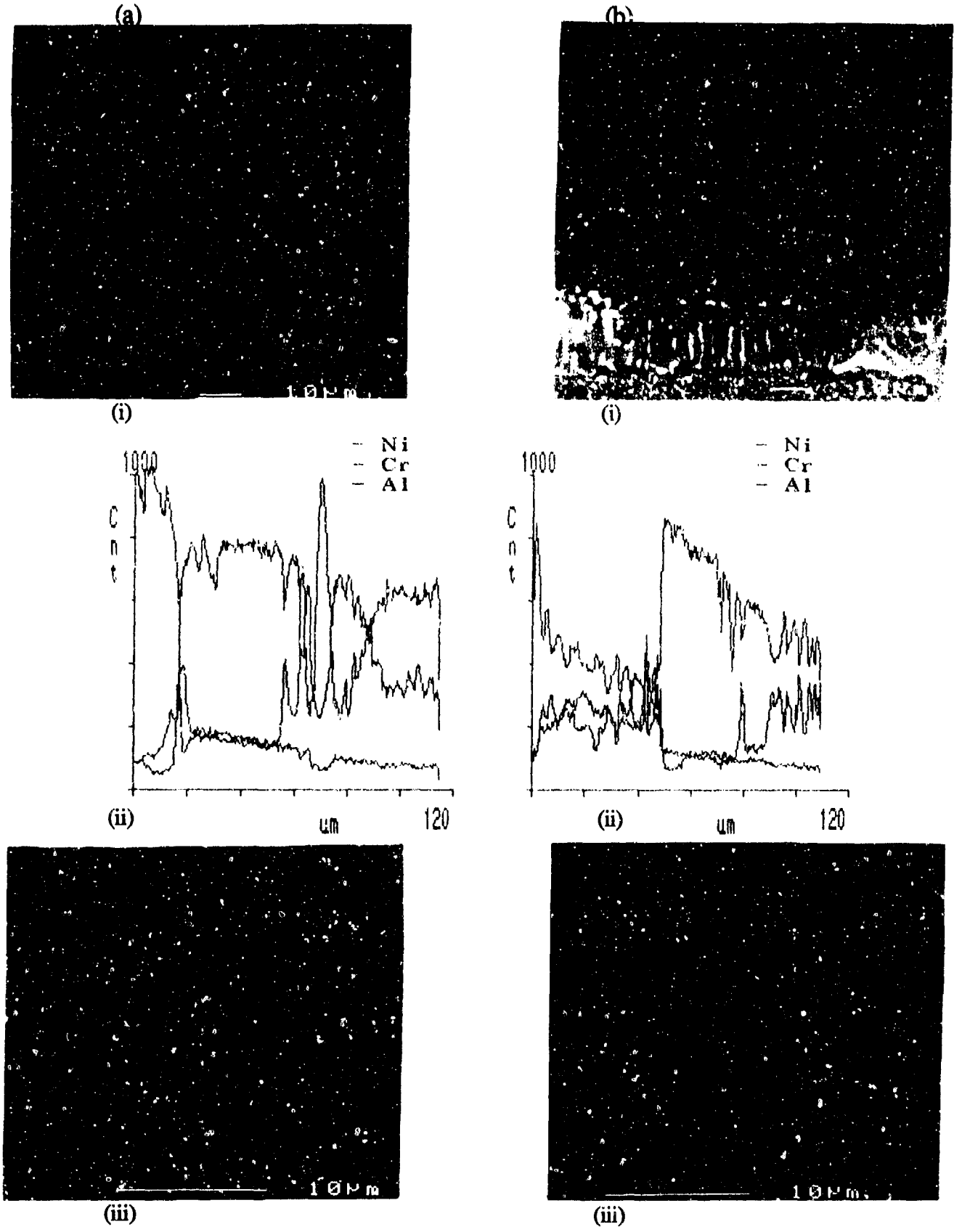

Figure 14 Platinum/rhodium-modified nickel aluminide (a) and a basic nickel aluminide (Type B) - (b) represented as micrographs at the concave leading edges (i) with corresponding line-scans (ii) and a magnified view of the corrosion front (iii).

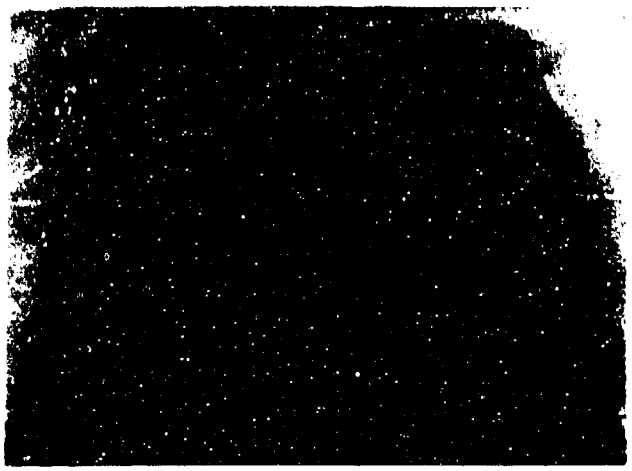

Figure 15 Severe hot corrosion attack of the uncoated internal cooling holes illustrating the importance of coating both the blade surface and cooling holes.

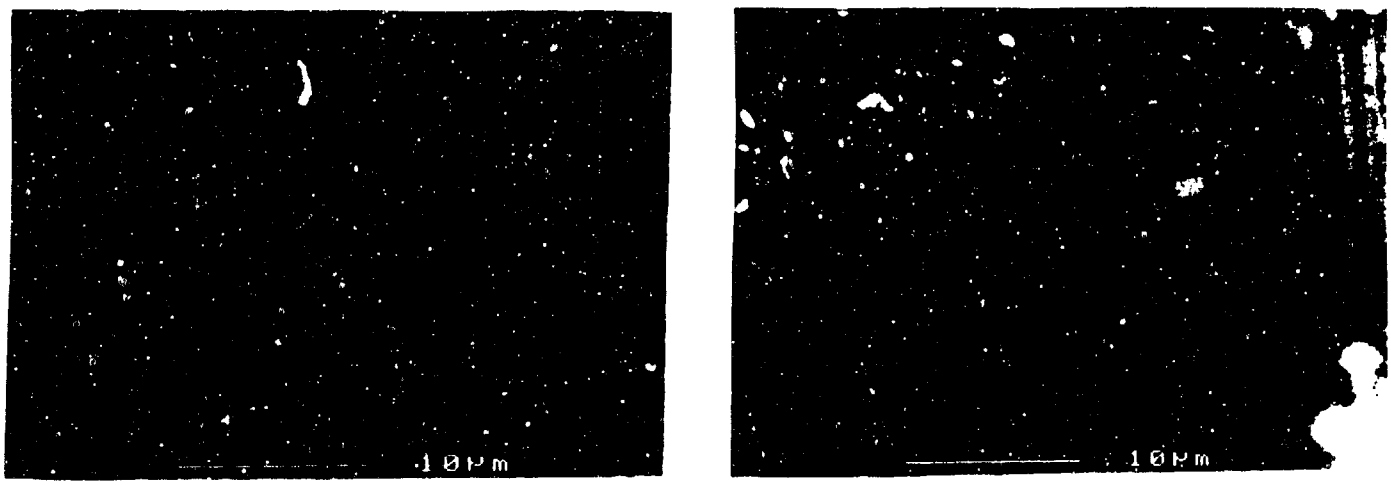

(a) (b)

Figure 16 Microsructures of the (a) platinum-modified aluminide and (b) silicon-modified aluminide coating just beneath the diffusion zone indicating the presence of the unfavourable needle-like sigma phase.

Table 1

RELATIVE DEGREES OF ATTACK FOR VARIOUS AREAS (MACROSCOPICALLY)

Type of Coating	Area 1	Area 2	Area 3	Area 4	Area 5	Area 6	Ψ
SI ALUMINIDE (1)	1	1	2	1	1	1	1.15
SI ALUMINIDE (2)	1	1	3	1	1	1	1.30
ALUMINIDE B (1)¥	2	1	3	1	2	2	1.73
ALUMINIDE A (1)	3	2	2	1	1	1	2.10
CR.ALUMINIDE (1)	2	3	3	3	2	1	2.50
PT/RH ALUMINIDE (1)¥	3	3	3	3	1	1	2.80
ALUMINIDE B (2)	4	2	4	2	1	2	2.95
CR ALUMINIDE (2)	3	4	4	3	1	1	3.20
PT/RH ALUMINIDE (2)	5	4	2	1	1	1	3.30
PT ALUMINIDE (1)	5	2	4	2	2	1	3.35
PT ALUMINIDE (2)	5	3	4	2	1	1	3.50
ALUMINIDE A (2)	5	3	3	3	2	2	3.60

- Areas are represented as follows:

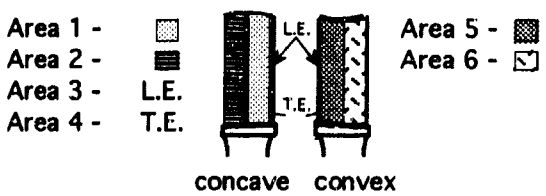

- Numbers under area columns represent relative degrees of attack for that specific area
  (1 - minimal attack 5 - maximum attack)

- Coatings are tabulated in decreasing order of their overall resistance to attack (Ψ)

- $\Psi = \sum_{i=1}^{6} WF_i \bullet DA_i$ $\{1 < \Psi < 5\}$

  where Ψ -parameter used to measure the blade's overall resistance to attack
  WF_i -weighting factor for area i $\{WF_i = 0.35\text{-}0.5(i\text{-}1)\}$
  DA_i -relative degree of attack for area i on a scale from 1 to 5

¥ These blades were handed over to the RAAF for reference and thus their respective investigations cease at this point..

Table 2

FOREIGN ELEMENTS PRESENT ON THE BLADES' SURFACES

Element	Extent	Possible sources for their presence
Iron	high	- iron based smoke suppressants (containing Fe_2O_3) - wear of iron based alloys further down the engine
Phosphorous	high	- constituent of proprietary platinum coating baths - lubricity improver/corrosion inhibitor (phosphate based) - phosphate containing fertilisers whilst low level flying
Sulfur	moderate	- fuel contaminant - sea salt (see Appendix II)
Calcium	high	- sea salt (see Appendix II) - water cleansing of blades
Potassium	small	- sea salt (see Appendix II)
Magnesium	moderate	- sea salt (see Appendix II)
Sodium	moderate	- sea salt (see Appendix II)
Silicon	high	- adherance of sand (SiO_2) whilst low level flying over shoreline or from landing on desert air strips
Zinc	small	- leaching out from the fuel tank lining

Table 3

OVERALL RANKING OF COATINGS

Type of coating	Average initial coating thickness (μm)†	Average final coating thickness (μm)	Coating loss(%)	Ranking
Pt/Rh mod.-aluminide (2)	85	55	35	1
Pt mod.-aluminide (1)	70	45	36	1
Si mod.-aluminide (1)	50	30	40	2
Si mod.-aluminide (2)	50	25	50	3
Pt mod.-aluminide (2)	70	25	64	4
Ni aluminide Type A (1)	85	30	65	4
Ni aluminide Type B (2)	80	10	88	5
Ni aluminide Type A (2)	85	breached	100	6
Cr mod.-aluminide (1)	65	breached	100	7
Cr mod.-aluminide (2)	65	breached	100	8

† From reference [1].

Element		Concentration (wt. %)
Nickel	(Ni)	balance
Chromium	(Cr)	16.0
Cobalt	(Co)	8.5
Aluminium	(Al)	3.4
Titanium	(Ti)	3.4
Tungsten	(W)	2.6
Molybdenum	(Mo)	1.75
Tantalum	(Ta)	1.75
Niobium	(Nb)	0.9
Iron	(Fe)	0.5 (a)
Silicon	(Si)	0.3 (a)
Manganese	(Mn)	0.2 (a)
Carbon	(C)	0.11
Zirconium	(Zr)	0.06
Boron	(B)	0.01

Appendix I Chemical composition of IN-738LC. +

\+ IN-738LC is a specification of Inconnel Alloy Corp.

(a) maximum composition.

	$g\ l^{-1}$	%
NaCl	23	52
$MgCl_2.6H_2O$	11	25
$Na_2SO_4.10H_2O$	8	18
$CaCl_2.2H_2O$	1·4	3
KBr, KCl	1·1	2
	44·5	100

Appendix II Typical composition of sea salt.

DISTRIBUTION

AUSTRALIA

Department of Defence

Defence Central

Chief Defence Scientist
AS, Science Corporate Management } shared copy
FAS Science Policy
Director, Departmental Publications
Counsellor, Defence Science, London (Doc Data sheet only)
Counsellor, Defence Science, Washington (Doc Data sheet only)
Scientific Adviser, Defence Central
OIC TRS, Defence Central Library
Document Exchange Centre, DSTIC (8 copies)
Defence Intelligence Organisation
Librarian H Block, Victoria Barracks, Melb (Doc Data sheet only)

Aeronautical Research Laboratory

Director
Library
Chief of Airframes and Engines Division
Author: S.G. Russo
N. Ryan
G. McAdam
P. Rohan

Materials Research Laboratory

Director/Library

Navy Office

Navy Scientific Adviser (3 copies Doc Data sheet only)
Director Aircraft Engineering - Navy
Naval Support Command
Superintendent, Naval Aircraft Logistics
Directorate of Aviation Projects - Navy
Director of Naval Supply - Aviation & Major Projects

Army Office

Scientific Adviser - Army (Doc Data sheet only)

Air Force Office

Air Force Scientific Adviser
Director General Engineering - Air Force
AHQ (SMAINTSO)
HQ Logistics Command (DGELS)
OIC ATF, ATS, RAAFSTT, WAGGA (2 copies)

Statutory and State Authorities and Industry

Aero-Space Technologies Australia, Systems Division Librarian
ASTA Engineering, Document Control Office
Ansett Airlines of Australia, Library
Australian Airlines, Library
Qantas Airways Limited
Civil Aviation Authority
Hawker de Havilland Aust Pty Ltd, Victoria, Library
Rolls Royce of Australia Pty Ltd, Manager

Universities and Colleges

NSW

Dr D.J. Young, School of Materials Science & Engineering

CANADA

NRC

J.H. Parkin Branch (Aeronautical & Mechanical Engineering Library)
Gas Dynamics Laboratory

FRANCE

ONERA

INDIA

Gas Turbine Research Establishment, Director

NETHERLANDS

National Aerospace Laboratory (NLR), Library

UNITED KINGDOM

Defence Research Agency (Aerospace)

Pyestock, Director

National Physical Laboratory, Library

Universities and Colleges

Cranfield Inst. of Technology

Library

UNITED STATES OF AMERICA

NASA Scientific and Technical Information Facility
Materials Information, American Society for Metals
United Technologies Corporation, Library

SPARES (5 COPIES)

TOTAL (56 COPIES)

AL 149 DEPARTMENT OF DEFENCE

DOCUMENT CONTROL DATA

PAGE CLASSIFICATION
UNCLASSIFIED

PRIVACY MARKING

1a. AR NUMBER	1b. ESTABLISHMENT NUMBER	2. DOCUMENT DATE	3. TASK NUMBER
AR-007-113	ARL-TR-2	NOVEMBER 1992	AIR 92/073

4. TITLE
FIELD EVALUATION OF SIX PROTECTIVE COATINGS APPLIED TO T-56 TURBINE BLADES AFTER 2000 HOURS OF ENGINE USE

5. SECURITY CLASSIFICATION (PLACE APPROPRIATE CLASSIFICATION IN BOX(S) IE. SECRET (S), CONF. (C) RESTRICTED (R), LIMITED (L) UNCLASSIFIED (U)).

DOCUMENT	TITLE	ABSTRACT
U	U	U

6. NO. PAGES
32

7. NO. REFS.
16

8. AUTHOR(S)
S.G. RUSSO

9. DOWNGRADING/DELIMITING INSTRUCTIONS
Not applicable.

10. CORPORATE AUTHOR AND ADDRESS
AERONAUTICAL RESEARCH LABORATORY
AIRFRAMES AND ENGINES DIVISION
506 LORIMER STREET
FISHERMENS BEND VIC 3207

11. OFFICE/POSITION RESPONSIBLE FOR:
SPONSOR RAAF
SECURITY -
DOWNGRADING -
APPROVAL CAED

12. SECONDARY DISTRIBUTION (OF THIS DOCUMENT)

Approved for public release.

OVERSEAS ENQUIRIES OUTSIDE STATED LIMITATIONS SHOULD BE REFERRED THROUGH DSTIC, ADMINISTRATIVE SERVICES BRANCH, DEPARTMENT OF DEFENCE, ANZAC PARK WEST OFFICES, ACT 2601

13a. THIS DOCUMENT MAY BE ANNOUNCED IN CATALOGUES AND AWARENESS SERVICES AVAILABLE TO . . . .

No limitations.

13b. CITATION FOR OTHER PURPOSES (IE. CASUAL ANNOUNCEMENT) MAY BE [X] UNRESTRICTED OR [ ] AS FOR 13a.

14. DESCRIPTORS
Protective coatings
Hot corrosion
Allison T56 engines
Gas turbine blades

15. DISCAT SUBJECT CATEGORIES
2105
1103

16. ABSTRACT
The first-stage high-pressure turbine blades in RAAF T-56 engines have a rejection rate which is unacceptably high. It has been revealed [1] that the current coating, a conventional nickel aluminide, has a greater than 60% rejection rate after 2000 hours. Consequently, a trial programme was established to assess the benefits of five alternative protective coatings and to determine which coatings, if any, could withstand up to 3000 engine operating hours. A previous report demonstrated the potential of platinum and platinum/rhodium modified aluminides after 1500 hours of engine operation. This report, after approximately 2000 hours of service, supports the previous recommendations that the precious metal aluminides offer superior resistance to hot corrosion than the conventional aluminides and chromium-modified aluminides. The inability of the silicon-modified aluminide to form an evenly distributed coating over the entire blade renders it unsuitable.

PAGE CLASSIFICATION UNCLASSIFIED
PRIVACY MARKING

THIS PAGE IS TO BE USED TO RECORD INFORMATION WHICH IS REQUIRED BY THE ESTABLISHMENT FOR ITS OWN USE BUT WHICH WILL NOT BE ADDED TO THE DISTIS DATA UNLESS SPECIFICALLY REQUESTED.

16. ABSTRACT (CONT).

17. IMPRINT

AERONAUTICAL RESEARCH LABORATORY, MELBOURNE

18. DOCUMENT SERIES AND NUMBER	19. COST CODE	20. TYPE OF REPORT AND PERIOD COVERED
Technical Report 2	33 340G	

21. COMPUTER PROGRAMS USED

22. ESTABLISHMENT FILE REF.(S)

23. ADDITIONAL INFORMATION (AS REQUIRED)